

1 The Quest for the Nuclear Equation of State

JÖRG AICHELIN AND JÜRGEN SCHAFFNER-BIELICH

1.1 Introduction

Theory predicts that hadronic matter at finite temperatures and densities has a rich structure. At moderate temperatures and densities, below the normal nuclear matter density, ρ_0 , there may be a liquid-gas phase transition above which nucleons are not bound anymore. With increasing temperature nuclear resonances and mesons appear and nuclear matter becomes hadronic matter. At a temperature between 165 and 195 *MeV* lattice gauge calculations predict (for zero chemical potential) a transition toward a plasma of quarks and gluons. For finite chemical potentials the transition temperature becomes even smaller.

Today it is still a challenge to confirm these predictions by experiments. Even the much simpler question "How much energy is needed to compress hadronic matter?" has, after 70 years of nuclear physics, not found a definite answer yet, despite of the importance of the answer not only for a fundamental understanding of hadronic matter but also for the understanding of many astrophysical observations. This search has been dubbed 'Quest for the hadronic equation of state' (EoS). Despite of progress in recent years neither the available data nor the theoretical approaches have surmounted the difficulties to come to indisputable conclusions for densities larger than the normal nuclear matter density.

One knows today that there are two possible means to explore the dependence of the compressional energy density E of hadronic matter on the density ρ and the temperature T , $E(\rho, T)$: heavy ion collisions and astrophysical observations. Until 1980 it was even debated whether in nuclear collisions matter becomes compressed but the experimental observation of the in-plane flow [1] and of the dependence of the π multiplicity on the centrality of the reaction [2] showed that nuclei react collectively and that matter becomes compressed during these reactions. Once the functional form of $E(\rho, T)$ is known the standard thermodynamical relations can be employed to study the other thermodynamical variables like pressure and entropy.

The $E(\rho, T)$ region which can be explored by astrophysical observations is, however, quite different from that accessible in heavy ion reactions. The astrophysical objects are usually cold whereas in heavy ion reactions compression goes along with excitation. Therefore a detailed knowledge of the entire $E(\rho, T)$ plane and hence of the hadronic interaction is necessary to compare astrophysical with heavy ion data.

If two nuclei collide with a high energy high densities can be achieved only for a very short time span ($\approx 10^{-23}s$). Thereafter the system expands and the density decreases rapidly. The first exploratory studies of such violent collisions between heavy nuclei have been carried out at the BEVALAC accelerator at Berkeley/USA, later the SIS accelerator at GSI/Germany and the AGS accelerator in Brookhaven/USA have continued and extended this research toward higher energies. Still higher energies are obtained at the relativistic heavy ion collider (RHIC) in Brookhaven/USA. Studies of the properties of hadronic matter at finite chemical potentials will be possible with the new FAIR project at GSI which will be operational in 2013.

On the experimental side there are only few observables which give directly access to the potential between nucleons. The measured scattering lengths allow to determine the nucleon-

nucleon potential in the different spin and isospin channels at low densities and, via the so-called ρt approximation, the binding energy at low densities. Weizsäcker has parameterized (above $A=40$ with a precision of 1%) the binding energies of stable nuclei by:

$$E = -a_V A + a_S A^{2/3} + a_C Z^2 A^{-1/3} + a_A \frac{(A - 2Z)^2}{A} + \lambda a_P \frac{1}{A^{3/4}}. \quad (1)$$

The first term with $a_V = 15.75 \text{ MeV}$ presents the volume energy, the second with $a_S = 17.8 \text{ MeV}$ the surface energy, followed by the Coulomb- and the symmetry energy with $a_C = 0.710 \text{ MeV}$ and $a_A = 23.7 \text{ MeV}$. The last term is the pairing energy with $a_P = 23.7 \text{ MeV}$ [3]. λ is $-1, 0, 1$ for odd-odd, odd-even and even-even nuclei, respectively. From this fit to data we can conclude that at ρ_0 the binding energy per nucleon in nuclear matter is $E/A = -15.75 \text{ MeV}$ and hence twice as large as the binding energy of finite nuclei.

On the theoretical side the difficulty to explore the density dependence of the compressional energy roots in three facts. First, it is a many body problem. With increasing density an increasing number of many-body Feynman diagrams has to be calculated. Second, the interaction between nucleons is exclusively phenomenological because it is not yet possible to link it to the fundamental theory of strong interaction, the Quantum Chromo Dynamics. The available data allow for different parameterizations which give, in turn, different density dependencies of the compressional energy. Third, the analysis of nucleon-nucleon scattering data reveals that the interaction has a hard core, i.e. that it becomes infinite or at least very large if the distance between the nucleons becomes smaller than $a = 0.4 - 0.5 \text{ fm}$. At intermediate distances the interaction is moderately attractive. Potentials based on meson exchange, like the Bonn or the Paris potential, allow to understand the interaction in terms of different mesons which are exchanged between the nucleons.

The hard core of the bare nucleon-nucleon interaction makes the usual concepts of many body physics, like the Hartree Fock mean field approach, inapplicable because the matrix elements diverge. The way out of this dilemma are so-called effective interactions, which are a partial resummation of many-body Feynman diagrams. The bare interaction is then simply the Born term of such a series.

The average internuclear distance d , given by

$$\frac{1}{d^3} = \rho = \frac{2k_F^3}{3\pi^2} \quad (2)$$

is at ρ_0 about three times as large as the hard core radius a . k_F is the wave number ($k_F = 1.42 \text{ fm}^{-1}$) at ρ_0 . Neglecting the moderate attraction at intermediate distances each hole line in the many-body Feynman diagrams contribute a factor $k_F a$ [4]. To describe nuclear matter it is therefore appropriate to resum those many-body diagrams which contain a minimal number of hole lines. They are presented on the left hand side of fig. 1.1.

This approach has been developed by Brückner and is called Brückner G-matrix approach [7]. Nonrelativistic calculations which use different parameterizations of the nucleon-nucleon potential produce results which all line up along the so-called Coester line, shown as NR on the right side of fig. 1.1. Obviously they reproduce neither the experimental nuclear matter binding energy marked by the rectangle nor the equilibrium density. Three body (or density dependent two body) potentials have to be added to bring the calculation in agreement with data but these additional potentials add also to the uncertainty of the calculations because their momentum as well as the density dependence of their strength is not well determined. Relativistic calculations improve the situation because the inherent production of virtual nucleon-antinucleon pairs acts like a repulsive interaction. Also they fall on a common line, marked by R in fig. 1.1. For the details of the many body approach to nuclear matter calculations we refer to the excellent review of Baldo and Maieron [8].

The state of the art many-body calculations agree relatively well at $\rho < \rho_0$ being constrained at $\rho \approx 0$ and at $\rho = \rho_0$, as discussed, but start to deviate substantially for $\rho > \rho_0$. This is shown in fig. 1.2, taken from [10], which displays the binding energy per nucleon for neutron matter and

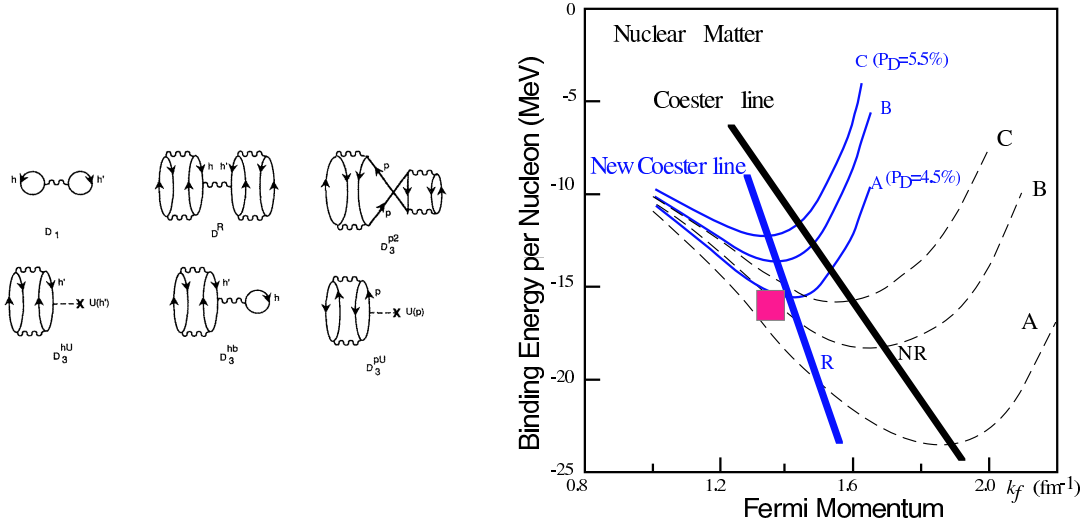


Figure 1.1: Left: Different diagrams which contribute to the many-body calculation of the ground state energy of nuclear matter [5]. Right: Binding energy per nucleons as a function of the Fermi momentum in many-body calculations, after [6].

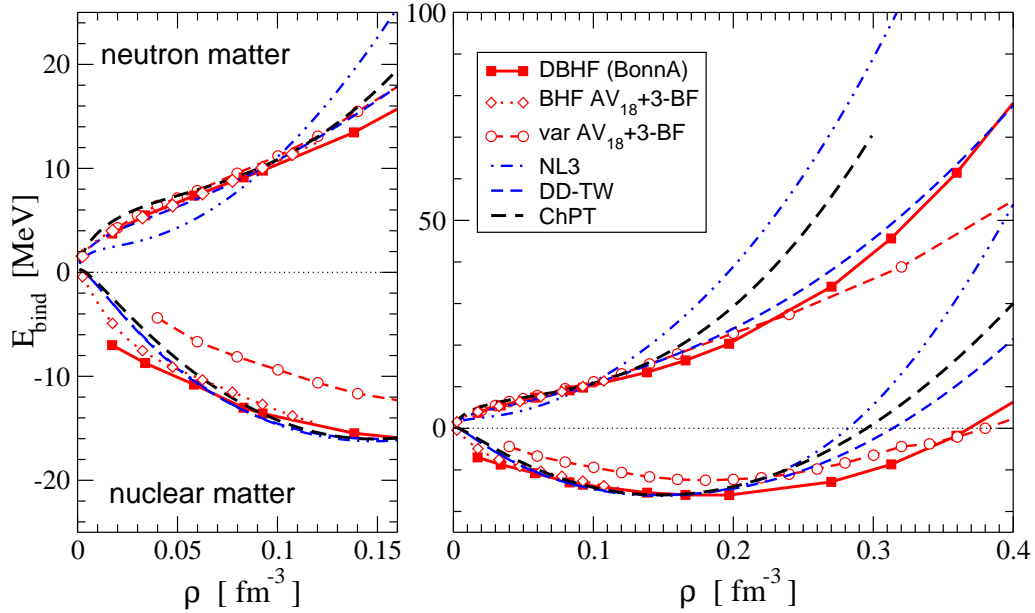


Figure 1.2: Binding energy per nucleon in nuclear matter and neutron matter. BHF/DBHF and variational calculations are compared to phenomenological density functionals (NL3, DD-TW) and ChPT+corr.. The left panel zooms the low density range. The figure is taken from ref. [9] where also the references to the different calculations can be found.

nuclear matter predicted by different approaches. It is evident from the figure that for $\rho > 1.5\rho_0$ the present theoretical uncertainty is as large as the binding energy per nucleon itself.

In order to make progress further experimental information is needed. Volume oscillations of nuclei [13, 14, 15, 16] would provide information on the curvature of the binding energy around the ground state density and hence allow the determination of the compressibility modulus

$$K = \frac{1}{\kappa} = -V \frac{dp}{dV} = 9\rho^2 \frac{d^2 E(\rho)/A}{(d\rho)^2} \Big|_{\rho=\rho_0} = R^2 \frac{d^2 E(\rho)/A}{dR^2}. \quad (3)$$

κ is the compressibility. Such a volume oscillation can be induced by the scattering of α particles. Their energy loss ΔE measures the excitation of the nucleus which is directly related to K by [11]

$$\Delta E = \sqrt{\frac{K}{m_N < r^2 >_A}} \quad (4)$$

where $< r^2 >_A$ is the squared radius of the nucleus and m_N the nucleon mass. A careful analysis of the excitations of different nuclei shows that the compressibility modulus has bulk, surface, Coulomb and pairing contributions, in analogy with the binding energy parametrization by Weizsäcker.

The values found for the volume compressibility in different non-relativistic and relativistic approaches are around $K = 240$ MeV [13, 14, 15, 16]. Very recently this value has been questioned because the influence of the surface compressibility has been underestimated [17]. This may cause an uncertainty of 30%.

The volume oscillations are, however, tiny and therefore information on the compressional energy for $\rho \gg \rho_0$ cannot be obtained by this method.

1.2 The EoS and Heavy-Ion Collisions

The only way to get on earth to densities well above ρ_0 are high energy heavy ion collisions. The challenge there is to identify those observables which carry information on the density and on the compressional energy which is obtained during the reaction and then to extract robust conclusions. To find these observables is complicated: The experimental results have to be compared with theoretical predictions calculated for different assumptions on the density and compressional energy. A prerequisite for such an approach are reliable simulation programs which make robust predictions.

The development of such programs faces a number of problems:

- a) heavy ions are not just a chunk of nuclear matter. Already the Weizsäcker mass formula tells us that surface effects are important.
- b) in heavy ion collisions compression is always accompanied by excitation which opens new degrees of freedom like resonance and meson production.
- c) the experimental spectra show that the system does not come even close to thermal equilibrium during the reaction.
- d) the time evolution of the reaction is strongly influenced by the production cross section for mesons and nuclear resonances and by the interaction among these particles. For many reaction channels the cross sections have not been measured and for many particles the interaction is not known.

In the last decades transport theories have been developed which cope with these challenges. Based on quantum molecular dynamics [18, 19, 20] or the quantum version of the Boltzmann equation [21, 22] these approaches simulate heavy ion reactions from the beginning, when projectile and target are still separated, to the end, when the particles are registered by the detectors. In the molecular dynamics approaches [18, 19, 20] nucleons are represented by Gaussian wave functions with a constant, time independent width. Hence the Wigner density of a nucleons reads as

$$f_i(\vec{r}, \vec{p}, t) = \frac{1}{\pi^3 \hbar^3} e^{-(\vec{r}-\vec{r}_i(t))^2 \frac{2}{L}} e^{-(\vec{p}-\vec{p}_i(t))^2 \frac{L}{2\hbar^2}}. \quad (5)$$

The total one particle Wigner density is the sum of the Wigner densities of all nucleons. The particles move according to Hamilton's equations of motion

$$\dot{r}_i = \frac{\partial \langle H \rangle}{\partial p_i} \quad \dot{p}_i = -\frac{\partial \langle H \rangle}{\partial r_i}. \quad (6)$$

The expectation value of the total Hamiltonian in this approach is approximated by

$$\begin{aligned} \langle H \rangle &= \langle T \rangle + \langle V \rangle \\ &= \sum_i \frac{p_i^2}{2m_i} + \sum_i \sum_{j>i} \int f_i(\vec{r}, \vec{p}, t) V^{ij} f_j(\vec{r}', \vec{p}', t) d\vec{r} d\vec{r}' d\vec{p} d\vec{p}' \quad . \end{aligned} \quad (7)$$

The baryon-potential consists of the real part of the G -Matrix which is supplemented by the Coulomb interaction between the charged particles. The former can be further subdivided in a part containing the contact Skyrme-type interaction only, a contribution due to a finite range Yukawa-potential, a momentum dependent part and a symmetry energy term depending of the difference between proton and neutron densities [18]. In infinite matter the interaction is reduced to

$$E/N = m_N + E_{kin} + \alpha \frac{\rho}{\rho_0} + \beta \left(\frac{\rho}{\rho_0}\right)^\gamma + S \frac{\rho}{\rho_0} \left[\frac{\rho_n - \rho_p}{\rho}\right]^2 + \epsilon f(p). \quad (8)$$

The imaginary part of G -Matrix acts as an elastic cross section which is complemented by inelastic cross sections.

This parametrization of the potential uses the minimal number of parameters because in infinite matter two of the three parameters α, β, γ are determined by the requirement that the binding energy is minimal at ρ_0 and equal to -15.75 MeV . The third parameter can be expressed in terms of the compressibility modulus K . This restrained ansatz is necessary as long as no observables have been identified which allow to fix further parameters like for example the (not necessarily linear) density dependence of the symmetry energy. $\epsilon f(p)$ is determined from optical potential measurements in p-A reactions.

For heavy ion collisions the situation is even more complicated because there is no constant density in the reaction zone and therefore the density has to be calculated by summing up the Wigner densities. The local density is therefore dependent on the width of the (Gaussian) wave functions, a parameter which is only vaguely controlled by nuclear surface properties.

In order to characterize the results the following strategy has been employed: The parameters of the two and three body interactions which are actually employed in the calculations, are fixed by the requirement that they agree in infinite matter with a given set of α, β, γ . This allows to characterize the potential parameters by a compressibility modulus: 'Soft' means $K=250 \text{ MeV}$ and 'Hard' means $K=380 \text{ MeV}$.

In the last two decades simulations using these transport theories became an indispensable tool to interpret the results of heavy ion collisions from $E_{kin} > 50 \text{ MeV}$ up to the highest beam energies. Because they predict the entirety of the experimental observables on an event by event basis, correlations can be identified and cross checks can be easily performed. These simulations have identified two observables which are sensitive to the compressional energy at $\rho \gg \rho_0$:

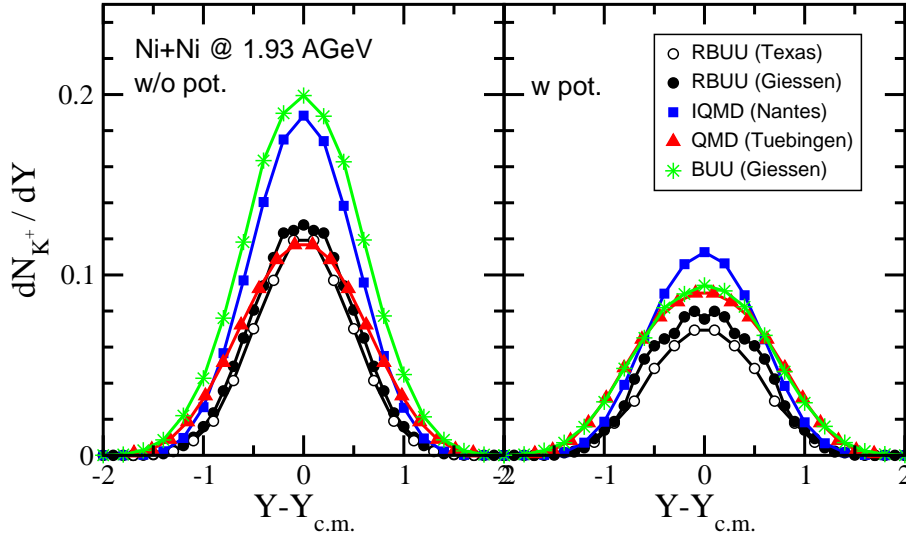


Figure 1.3: K^+ rapidity distributions in central ($b=1$ fm) Ni+Ni reactions at 1.93 AGeV from various transport models in their default versions: RBUU (Texas, open circles), RBUU (Giessen, full circles), IQMD (Nantes, full squares), QMD (Tübingen, full triangles) and BUU (Giessen). The left figure shows results without kaon in-medium potentials while the right one includes potentials. The figures are taken from refs. [25, 26].

- a) the in-plane flow of nuclei in semi-central heavy ion collisions
- b) the production of K^+ mesons at subthreshold and threshold energies.

For semi-central collisions already hydrodynamical calculations have predicted an in-plane flow. The transport theories allowed for a quantitative prediction of this collective phenomenon. For a review we refer to [23]. When two nuclei collide the interaction zone has a higher density than the surrounding spectator matter. The density gradient creates an energy gradient and hence a force, \mathbf{F}_e (see eq. 8). \mathbf{e} lies (almost) in the reaction plane and is (almost) perpendicular to the beam direction: $\mathbf{e} = e_x$. The force changes the momentum of the nucleons at the interface between participant and spectator zone by

$$\Delta p_x \approx \frac{dV(x)}{dx} r_0 A^{1/3} \frac{m_N}{\langle p_z^{cm} \rangle} \quad (9)$$

where $\langle p_z^{cm} \rangle$ is the momentum of a nucleon in beam direction in the center of mass system and $r_0 A^{1/3}$ the length of the nucleus. The nucleons at the surface of the interaction zone, where $|\frac{dV(x)}{dx}|$ is largest, transfer this momentum to the nucleons which are around creating a collective in-plane flow. For projectile and target nucleons the momentum transfer is of opposite direction and can be measured because projectile (target) nucleons end up at forward (backward) rapidity. It is evident from eq. (9) that Δp_x depends via $\frac{dV(x)}{dx}$ on the compressional energy and the simulation programs have verified this dependence. The difficulty is that $\langle \Delta p_x \rangle$ is tiny and the difference of $\langle \Delta p_x \rangle$ for different parameterizations of the compressional energy is even smaller. A quantitative prediction depends crucially on the ability of the simulations programs to simulate very accurately not only the bulk but also the properties of the surface where $\frac{dV(x)}{dx}$ is largest. Presently the tiny difference of $\frac{dV(x)}{dx}$ for two different equations of state in one program is smaller than the difference of $\frac{dV(x)}{dx}$ between two different programs which use the same EoS and which predict the same bulk properties. Therefore it is premature to make quantitative predictions of the compressional energy based on the observed in-plane flow [24].

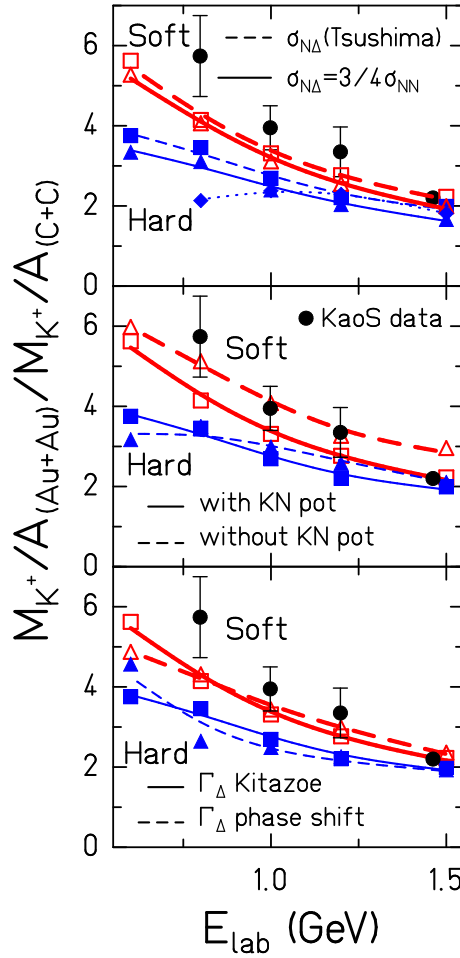


Figure 1.4: Comparison of the measured excitation function of the ratio of the K^+ multiplicities per nucleon obtained in Au+Au and in C+C reactions (Ref. [31]) with various calculations. Results of simulations with a hard EoS are shown as thin (blue) lines, those with a soft EoS by thick (red) lines. The calculated values are given by symbols, the lines are drawn to guide the eye. On top, two different versions of the $N\Delta \rightarrow K^+\Lambda N$ cross sections are used. One is based on isospin arguments [29], the other is determined by a relativistic tree level calculation [30]. Middle: IQMD calculations with and without KN potential are compared. Bottom: The influence of different options for the life time of Δ in matter is demonstrated. The figure is taken from ref.[27].

For the second method to study compressional energies at high densities, on the contrary, the results of different simulation programs have converged [25, 26]. This is shown in fig. 1.3 where the K^+ rapidity distributions for central ($b=1$ fm) Ni+Ni reactions at 1.93 AGeV from various transport models are displayed. The different results in their default versions come from different assumption on only vaguely known input quantities: The $N\Delta$ cross section, the Δ lifetime in matter and the strength of the KN potential. Once the same input is used the results agree quite well.

K^+ mesons produced far below the NN threshold cannot be created in first-chance collisions between projectile and target nucleons. They do not provide sufficient energy even if one includes the Fermi motion. The necessary energy for the production of a K^+ meson in the NN center of mass system is 671 MeV because in addition to the production of a kaon a nucleon has to be converted into a Λ to conserve strangeness. Before nucleons can create a K^+ at these subthreshold energies, they have to accumulate energy. The most effective way to do this is to convert a nucleon into a Δ and to produce in a subsequent collision a K^+ meson via $\Delta N \rightarrow NK^+\Lambda$. Two effects link the yield of produced K^+ with the density reached in the collision and the stiffness of the compressional energy. If less energy is needed to compress matter (i) more energy is available for the K^+ production and (ii) the density which can be reached in these reactions will be higher.

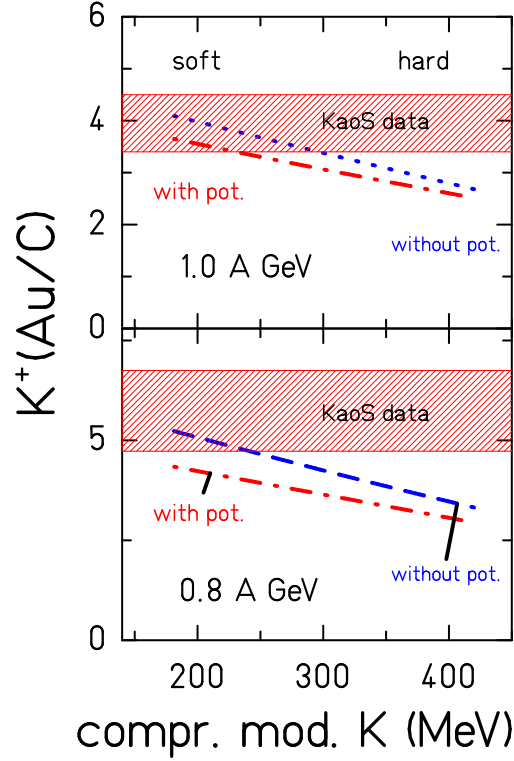


Figure 1.5: The double ratio $[M/A(\text{Au}+\text{Au})]/[M/A(\text{C}+\text{C})]$ calculated within the IQMD model (with and without KN potential) as a function of K for two beam energies, 0.8 (top) and 1.0 AGeV (bottom). The experimental values are given as a band and allow to estimate upper limits for the compressibility modulus K as described in the text.

Higher density means a smaller mean free path and therefore the time between collisions becomes shorter. Thus the Δ has an increased chance to produce a K^+ before it decays. Consequently, the K^+ yield depends on the compressional energy. At beam energies around 1 AGeV matter becomes highly excited and mesons are formed. Therefore this process tests highly excited hadronic matter. At beam energies > 2 AGeV first-chance collisions dominate and this sensitivity is lost. The simulations verify that the K^+ in Au+Au collisions at 1.5 AGeV are indeed produced at around $2\rho_0$ [27].

The K^+ mesons behave as a quasi particle even at high densities [28] and can therefore be propagated as the baryons in these simulations programs. The largest uncertainty of the K^+ production in heavy ion collisions is the only theoretically calculated ΔN production cross section [29, 30] which is dominating. Its influence on the observables can be minimized by analyzing ratio of the multiplicity in light and heavy symmetric systems. It is further constrained by the excitation function of the K^+ multiplicity. This ratio is displayed in fig. 1.4. All three graphs show calculations with a soft and a hard EoS. For the three calculations little known or unknown input parameters are varied ($N\Delta$ cross section, top, KN potential, middle, and Δ life time, bottom) to see whether the conclusion is robust. We see that different assumptions on these input quantities do not invalidate the conclusion that the data are incompatible with the assumption that the EoS is soft.

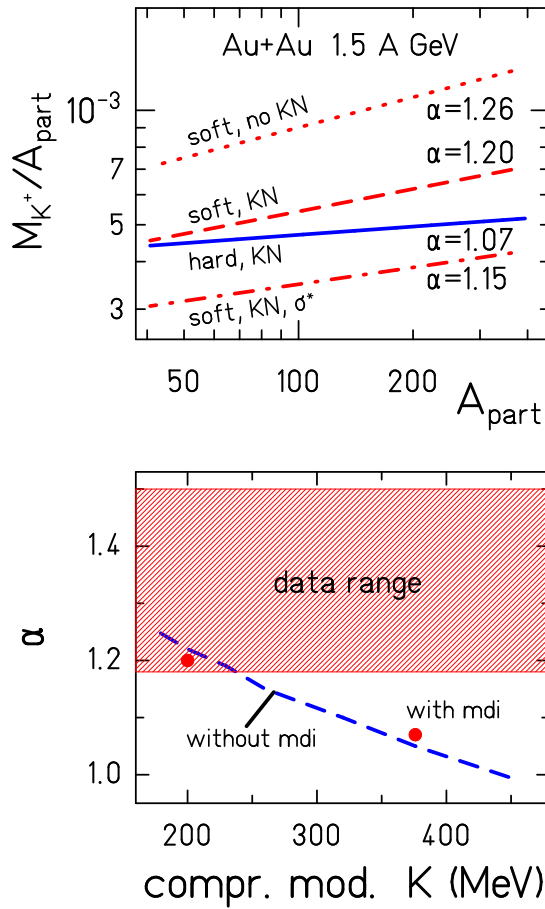


Figure 1.6: Dependence of the K^+ scaling on the EoS. We present this dependence in form of $M_{K^+} = A_{\text{part}}^\alpha$. On the top the dependence of M_{K^+}/A_{part} as a function of A_{part} is shown for different options: a hard EoS with KN potential (solid line), the other three lines show the result for a soft EoS, without KN potential and $\sigma(N\Delta)$ from Tsushima [30] (dotted line), with KN potential and the same parametrization of the cross section (dashed line) and with KN potential and $\sigma(N\Delta) = 3/4\sigma(NN)$. On the bottom the fit exponent α is shown as a function of the compressibility modulus for calculations with momentum-dependent interactions (mdi) and for static interactions ($\epsilon=0$, dashed line).

Fig. 1.5 shows the double ratio as a function of the compressibility modulus K for two beam energies with and without KN potential. Also for this observable data are not compatible with a hard EoS.

This conclusion is confirmed by another, independent observable, the centrality dependence of the K^+ production. It can be described by $M_{K^+} \propto A_{\text{part}}^\alpha$. The value of α depends on the choice of the input parameter, as shown in fig. 1.6, top. Again, only a soft EoS can describe the data, as can be seen in the bottom part, where we display the result with and without a momentum dependent interaction ($\epsilon = 0$ in eq. 8).

Thus heavy ion reactions, in which densities up to $3\rho_0$ are obtained and in which almost all K^+ are produced at densities well above ρ_0 , the experimental results are only compatible with a soft EoS. The value of K obtained from high energy heavy ion collisions agrees well with that extracted from the analysis of density vibrations around ρ_0 . This has to be considered as accident because the density dependence of the compressional energy can be more complicated than suggested by the simple parametrization of eq. 8. The precision of present day experiments and theory does not allow for a determination of more than one parameter which has been traditionally expressed as the compressibility modulus K at ρ_0 . One has to keep in mind that in heavy ion reactions this value of K has been extracted in a complicated way from a very excited non equilibrium system where mesons and nuclear resonances are present. Conclusions on the compressibility modulus of nuclear matter at large densities and a small temperature have therefore to be drawn with great caution. Nevertheless, this analysis presents presently the only robust information on the compressional energy of hadronic matter well above normal nuclear matter density which has been obtained from heavy ion experiments.

1.3 The EoS and Astrophysics

The nuclear equation of state as determined from heavy-ion experiments has crucial impacts in high-density astrophysics in particular on the physics of neutron stars, core-collapse supernovae, and neutron star mergers.

Neutron stars are the final endpoint of stellar evolution of stars more massive than about eight solar masses. Those stars end in a spectacular core-collapse supernova which outshines for a brief moment of time even the light of an entire galaxy. Matter is compressed to extreme densities, energy densities above normal nuclear matter density are reached in the collapse of the degenerate core of the supermassive progenitor star. Only the strong repulsive interactions between nucleons can prevent the further collapse to a black hole providing the enormous pressure necessary to withstand the pull of gravity. A stable proto-neutron star is formed with initial temperatures of about 20 to 50 MeV. It is important to realize that the degeneracy pressure alone is not enough to ensure the stability of the proto-neutron star, it is essential that the nuclear equation of state controls the bounce back of material during the collapse of matter. A shock wave is built up due to the strong repulsion of nucleons which is moving outwards. The stable hot proto-neutron star cools down within about one minute by the emission of neutrinos from its surface which have been traveling by a random walk from the core. The temperature drops down to less than 1 MeV within that first minute. The temperature is now so low in comparison to the Fermi energy of the nucleons in the core region, that temperature effects can be safely ignored afterwards. A cold neutron star is born which is still emitting neutrinos in a wind.

1.3.1 The nuclear EoS, supernovae and neutron star mergers

The conventional mechanism to be believed to be responsible for a successful explosion is the so called neutrino driven explosion [32] which happens on a timescale of less than a second after the bounce. The shock wave generated by the bounce of matter is not energetically enough to plow through all the material of the progenitor star and stalls at a few hundred kilometers. The neutrinos emitted from the hot proto-neutron star carry an enormous energy, in total 10^{53} erg, which is about two orders of magnitudes larger than the energy contained in the outflowing material of observed supernovae. Therefore, if just a small fraction of the energy of neutrinos is transferred to the stalled shock front, it could be revived so that a successful explosion occurs.

However, until recently, no successful explosion could be achieved even with improved models, in particular with respect to the treatment of the propagation of neutrinos. One dimensional supernova simulations were inherently unsuccessful in achieving sufficient explosion energies so far. New mechanisms have been suggested for a successful supernova explosion as the standing accretion shock instability (SASI) [33, 34] or acoustic oscillations from the proto-neutron star [35], which were observed when treating the dynamics of supernova evolution in unconstrained multi-dimensional simulations. The results demonstrate that nonradial hydrodynamic instabilities, which can help to support explosions, depend on the underlying nuclear equation of state [33]. In particular, the stiffness of the nuclear equation of state affects the time variability on the neutrino and gravitational wave signal with larger amplitudes as well as higher frequencies for more compact newly born neutron stars. Information on the nuclear equation of state is therefore inherently imprinted on the neutrino and gravitational wave emission [36]. For simulations taking into account rotation, the effects of the nuclear equation of state on these astrophysical observables seems to be much smaller though [37].

The present situation is described poignantly by the final statement in the abstract of the recent review on the theoretical status of core-collapse supernovae in ref. [38]: ‘The explosion mechanism of more massive progenitors is still a puzzle. It might involve effects of three-dimensional hydrodynamics or might point to the relevance of rapid rotation and magnetohydrodynamics, or to still incompletely explored properties of neutrinos and the high-density equation of state.’

Also for neutron star mergers as well as collisions of neutron stars with black holes impacts of the nuclear equation of state have been observed in numerical simulations. In [39, 40], it was found that the amount of material loss to the interstellar medium for merging neutron stars depends strongly on the stiffness of the nuclear equation of state with corresponding implications for element synthesis in the r-process. The peak in the gravitational wave spectrum is highly sensitive to the nuclear equation of state and on the total mass of the binary system. The total mass of the binary neutron star system could be determined from the inspiral chirp signal so that the frequency of the postmerger signal serves a sensitive indicator of the properties of the high-density nuclear equation of state [41, 42]. For neutron stars being swallowed by black holes the complete dynamics is governed by the mass loss and how the neutron star reacts to it. A stiff equation of state causes an episodic mass transfer over many orbits which is visible in the gravitational wave signal. On the contrary, for a soft polytropic equation of state it was observed that the neutron star was ripped apart at the first encounter with the black hole [43, 44].

All of the above mentioned newer investigations have been performed with basically two different nuclear equation of state which are constructed in such a way that they are suitable for astrophysical applications: the one of Lattimer and Swesty [45] with a Skyrme-type interaction and the one by Shen et al. [46] using a relativistic mean-field theoretical model. Both of them are purely nucleonic in nature and at present the only ones available in the modern literature. Astrophysical studies of the effects from quark matter have been hampered by this fact and only a few exploratory investigations have been performed. In ref. [47] neutron star mergers have been calculated with the use of a simple quark matter equation of state. Effects from the presence of quark matter have been seen in the collapse behavior of the merger remnant and in the gravita-

tional wave signal. In ref. [48] the formation of quark matter produced a second shock wave but the calculation was performed without any neutrino transport. The failed explosion and the collapse of heavy progenitor stars to a black hole have been studied in ref. [49, 50] with effects of a phase transition to quark matter. Quark matter appeared at quite high densities so that that collapse to a black hole could not be stopped and happened even faster than for the case without quark matter. No second shock wave has been seen in these simulations.

Recently, it was demonstrated in a detailed one-dimensional computation with full treatment of the neutrino transport that the formation of a quark-gluon plasma shortly after bounce produces an accretion shock at the surface of the quark matter core [51]. The second shock front travels outwards and is so energetic that it passes over the stalled first shock and achieves a successful explosion with quite large explosion energies. The presence of the second shock can be observed from the temporal profile of the neutrino emission from the supernova. The first shock from the bounce of nuclear matter produces a peak of neutrinos as the matter is neutronized. A second neutrino burst is generated by the emission of antineutrinos when the second shock formed from the quark matter core runs over hadronic matter and neutrons are transformed back to protons. This second peak in the neutrino spectra serves as a signal for the presence of a strong phase transition, the time delay compared to the first neutrino peak and the height of the peak gives insights onto the location and the strength of the phase transition line in the QCD phase diagram.

1.3.2 The nuclear EoS and compact stars

The mass-radius curve of neutron stars formed in core-collapse supernovae is entirely determined by the nuclear equation of state, with only minor corrections from rotation. The basic structure equations in spherical symmetry for compact stars are given by solving the equations of General Relativity for a static and spherically symmetric metric and result in the Tolman-Oppenheimer-Volkoff (TOV) equations [52, 53, 54]

$$\frac{dP}{dr} = -G \frac{M_r \epsilon}{r^2} \left(1 + \frac{P}{\epsilon}\right) \left(1 + \frac{4\pi r^3 P}{M_r}\right) \left(1 - \frac{2GM_r}{r}\right)^{-1}$$

with the mass conservation equation

$$\frac{dM}{dr} = 4\pi r^2 \epsilon$$

There are three relativistic correction factors compared to the Newtonian expression for the hydrodynamic structure equations for ordinary stars. One corrections factor is present for the mass M_r contained within the radius r and one for the energy density, where effects from the pressure are taken into account. The third correction factor originates from the outside solution and modifies the radius with the Schwarzschild factor, in particular close to the Schwarzschild radius $R_s = 2GM$ where M is the total gravitational mass of the star.

The maximum mass of white dwarfs is controlled by the Fermi pressure of electrons. It is well known that the maximum mass of a neutron star must be determined by the repulsive nature of the nuclear force, not by the Fermi pressure of nucleons. The maximum mass of a neutron star just supported by Fermi degeneracy pressure of a free gas of neutrons results in a maximum mass of just $0.7M_\odot$ [54]. The mass of the Hulse-Taylor pulsar has been measured to be $(1.4414 \pm 0.0002)M_\odot$ [55], which is more than a factor two larger. Such a large neutron star mass can only be explained by including effects from strong interactions. One can adopt an inversion procedure, as first outlined by Gerlach [56], which relates the mass-radius curve of neutron stars to the underlying nuclear equation of state [57]. Hence, the knowledge of the masses and radii of compact stars gives immediately a unique constraint on the properties of dense nuclear matter.

In the near future, one could not only derive properties of matter under extreme conditions by spectroscopy or by the detection of neutrinos but also by 'listening' to astrophysical events

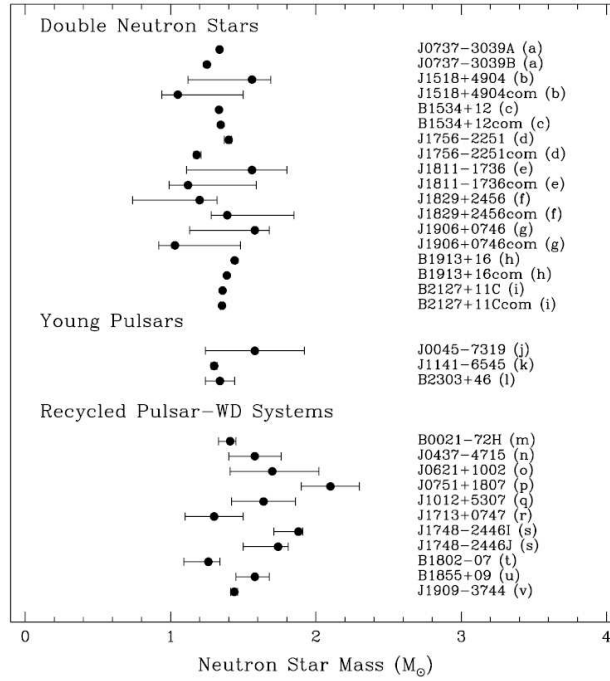


Figure 1.7: Mass measurements from pulsars, rotation-powered neutron stars (taken from [59]). Note that the mass of the pulsar PSR J0751+1807 has been corrected from $M = (2.1 \pm 0.1)M_{\odot}$ downwards to $(1.26 \pm 0.14)M_{\odot}$, see [60].

by the detection of gravitational waves. If there exists a rigid phase in the core of neutron stars, pulsars could pertain a slight deformation so that they wobble thereby emitting characteristic gravitational waves. More spectacular signals are expected from the merging of two neutron stars. Several double neutron star systems have been discovered in our galaxy, the best known is the Hulse-Taylor binary pulsar PSR 1916+13. Gravity is so strong in those double neutron star systems, that a significant amount of energy is lost by the emission of gravitational waves. The two neutron stars spiral inwards and are prone to collide with each other in a spectacular astrophysical event. The gravitational wave signal consists basically of three parts. First a rising chirp occurs just before the two neutron stars merge which is determined by the compactness of the neutron stars, the ratio of the mass to radius. The middle part is controlled by the nuclear equation of state where the actual merger of the two neutron stars is happening. Finally, the system collapses to a deformed black hole which is ringing down by the emission of gravitational waves. The middle part of the gravitational wave pattern is the least well known due to our limited knowledge of the high-density nuclear equation of state. However, this fact serves as an opportunity to learn more about it by measuring gravitational waves. Today several gravitational wave detectors are in operation, as LIGO, VIRGO, TAMA, GEO600. The LIGO collaboration just published new limits on the emission of gravitational waves from the observation of pulsars which are now at the so-called spin-down limit [58]. Pulsars can lose their rotational energy and spin-down by either the emission of electromagnetic radiation or by gravitational waves. LIGO is now at the limit to measure gravitational waves of the energy scale given by the loss of rotational energy of the crab pulsar. In just a few years LIGO will enhance its sensitivity by a few factors with the LIGO+ upgrade and advanced LIGO, so that the possible emission of gravitational waves from single wobbling pulsars can be tested.

There are more than 1700 pulsars, rotation-powered neutron stars, discovered within our local group of galaxies as listed in the ATNF pulsar database [61]. Several binary systems are known,

where a neutron star has a companion, be it a main-sequence star, a white dwarf or another neutron star. For one system, the double pulsar J0737-3039A/B, the radio pulses of both neutron stars have been detected [62]. The masses of pulsars are determined by measuring corrections from General Relativity for the orbital parameters as deduced from the timing of the pulsar's radio signal. Compilations of neutron star masses have found a rather narrow range of 1.35 ± 0.05 [63]. Fig. 1.7 shows a recent compilation of pulsar mass measurements from [59]. The smallest neutron star mass measured so far is $M = (1.18 \pm 0.02)M_\odot$ for the pulsar J1756-2251 [64], the heaviest most reliably determined at present is the one of the Hulse-Taylor pulsar with $(1.4414 \pm 0.0002)M_\odot$ [55].

In recent pulsar observations [59] much larger values than have been reported but have to be taken with caution. The mass of the pulsar J0751+1807 was corrected from $M = (2.1 \pm 0.1)M_\odot$ [65] to $(1.26 \pm 0.14)M_\odot$ as new data became available [60]. The mass of the neutron star in Vela X-1 has been extracted to be not less than $(1.88 \pm 0.13)M_\odot$ for an inclination angle of 90 degrees, which relies on the radial velocity measurement of the optical companion star with possible systematic errors [66]. There are a series of measurements of extremely massive pulsars in globular clusters, where just the periastron advance has been determined but not the inclination angle of the orbit [67, 68, 69]. For the pulsar PSR J1748-2021B a mass of $(2.74 \pm 0.21)M_\odot$ is reported by using a statistical analysis for the inclination angle [68]. We stress that this is not a direct mass measurement and that a second relativistic correction from General Relativity has to be determined before one can draw any conclusion about the true pulsar mass. There is a recent mass measurement by a highly excentric pulsar, PSR J1903+0327, with $(1.74 \pm 0.04)M_\odot$ [70], but over only a time period of 1.5 years so that possible effects from proper motions affecting the mass measurement can not be excluded. The other high mass measurement reported for the pulsar J0437-4715 of $M = (1.76 \pm 0.20)M_\odot$ [71] has a lower 2σ bound than the one of the Hulse-Taylor pulsar.

The determination of the mass-radius relation of a neutron stars are model dependent so far. The outermost layer of the neutron star, the atmosphere, needs to be modeled in order to fit to the observed x-ray spectra. Presently, the atmosphere of isolated neutron stars is not understood, as the optical flux is not compatible with an extrapolation of the observed x-ray spectra. The extracted radius is the one as observed by an observer at infinite distance to the neutron star and is defined by the true radius and the mass of the star as

$$R_\infty = \frac{R}{\sqrt{1 - R_s/R}} \quad (10)$$

with the Schwarzschild radius $R_s = 2GM$. The most prominent example is the isolated neutron star RXJ1856.5-3754 for which a constraint on the radiation radius of $R_\infty > 17$ km ($d/140pc$) was inferred [72, 73]. For the given redshift of $z \approx 0.22$ this radiation radius results in $M \approx 1.55M_\odot$ and $R = 14$ km. The largest error resides in the distance d of the pulsar to Earth, so that in principle any mass between $1.1M_\odot$ and $2M_\odot$ with radii of 10 km and 18 km, respectively, seems possible.

Accreting neutron stars can be sources of x-ray bursts as matter is heated up during accretion and falls onto the neutron star. For the x-ray burster EXO 0748-676 redshifted spectral lines have been extracted in the aftermath of an x-ray burst [76] seemingly originating from the surface of the compact star. Follow-up observations of another burst in 2003 could not confirm this finding [77]. A model analysis of the x-ray burst led to rather tight constraints for the mass and radius of the compact star of $M \geq (2.10 \pm 0.28)M_\odot$ and $R \geq (13.8 \pm 1.8)$ km [78] which are based on the redshift measurement of [76]. However, a detailed multiwavelength analysis concluded that the mass of the compact star is more compatible with $1.35M_\odot$ than with $2.1M_\odot$ [79]. In any case, compact star masses and radii constraints as given by [78] still allow for the possible existence of quark matter in the core of the compact star [80] contrary to the strong claims made in [78]. Spectral fits to accreting neutron stars in quiescence were hampered by the fact that the surface gravity of the neutron stars was not adjusted consistently but was fixed. Starting with ref. [81] consistent

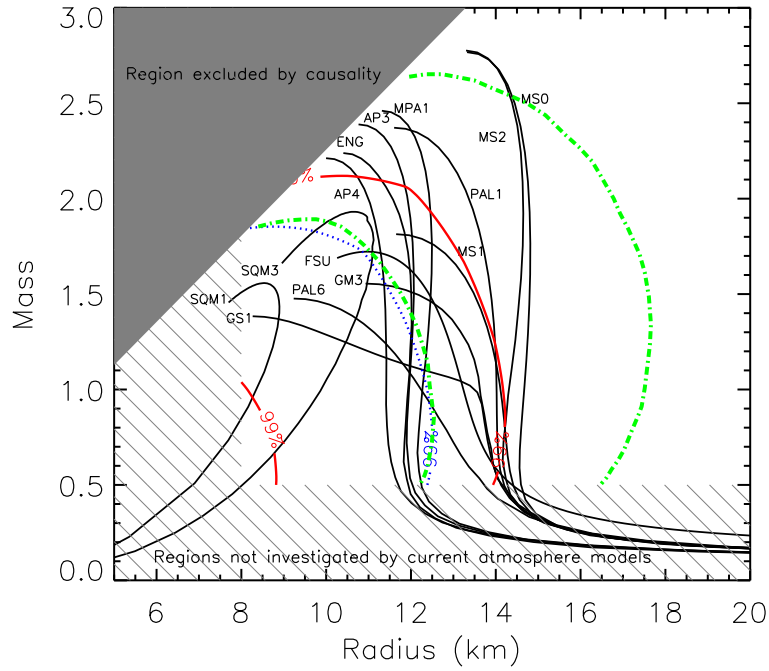


Figure 1.8: Mass-radius constraints from spectral modeling of pulsars in globular clusters (from [74]). The mass-radius curve has to pass through the region bounded by the two lines. Three different mass-radius constraint have been shown for neutron stars in the globular cluster M13 (dotted line), in ω Cen (solid lines) and for X7 in 47 Tuc (dash-dotted lines). The various mass-radius curves for different nuclear equation of states shown are taken from [75]. The curves starting from the origin are for pure quark stars without an hadronic mantle which are selfbound.

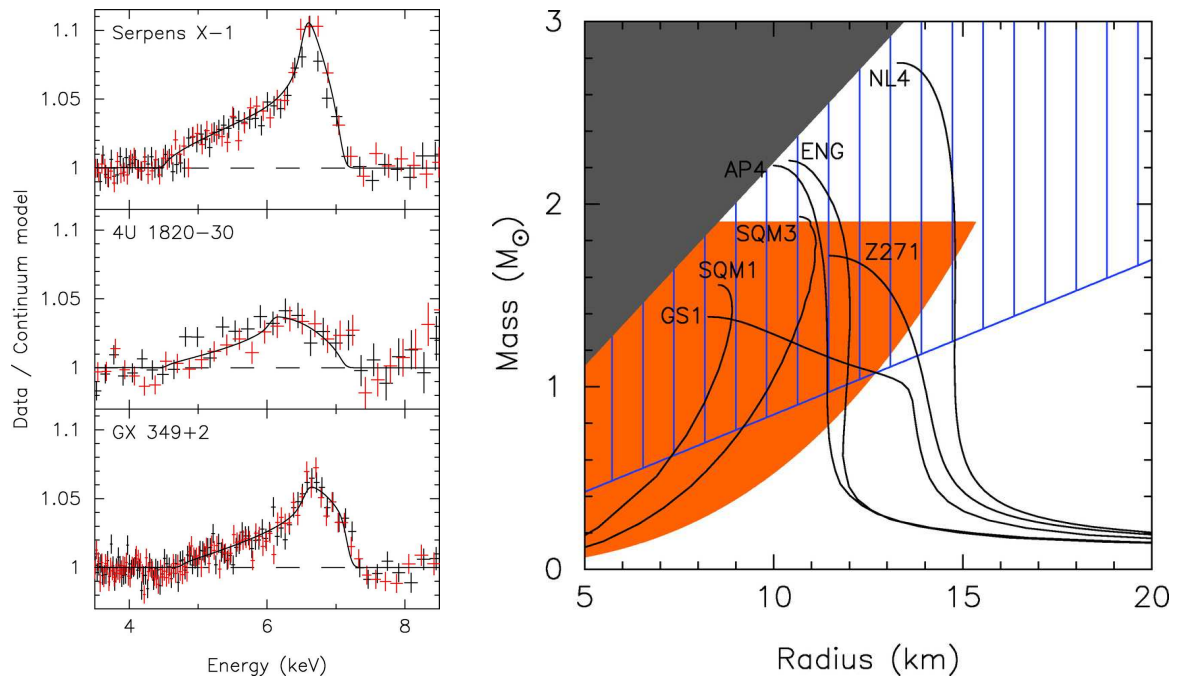


Figure 1.9: Left: Redshifted iron lines from several low-mass x-ray binaries. Right: Constraint on the mass-radius relation for neutron stars from the maximum redshift measured for the iron lines, indicated by the striped region. The pie-shaded filled area is the region in mass and radius compatible with the measurements of quasi-periodic oscillations (QPOs) of accreting neutron stars (figures are taken from [82]).

spectral fits became available, first applied to the neutron star X7 in the globular cluster 47 Tuc. The constraint on the mass and radius of the neutron star are quite loose. The authors quote strong limits for the mass by fixing the radius and vice versa which should be taken with care. A glance at their exclusion plot shows that for a radius of $R \approx 14$ km any mass between $0.5M_\odot$ and $2.3M_\odot$ is allowed by the fit. Spectral modeling of the neutron stars in ω Cen and M13 can be found in [74] with similarly large errors. Note, that the combination of several spectral modeling results on the constraint for the mass-radius relation of neutron stars that the mass-radius curve has to pass through all the different regions allowed by the spectral fits somewhere and not that the curve has to strike the common area of all fits. The spectral fit of the neutron star in M13 demands that the radius should be smaller than about 12 km with a mass smaller than $1.8M_\odot$ on the 99% confidence level (see fig. 1.8).

Interestingly, there are constraints on the radius of the neutron star which mostly rely on General Relativity. A broadened iron-line characteristic for redshifted iron-lines from an accretion disk have been measured for three low-mass x-ray binaries [82]. The lower endpoint in the energy of the broadened line determines the maximum redshift and therefore the inner radius of the accretion disk relative to the Schwarzschild radius of the neutron star. It turned out that neutron stars should have a radius smaller than $R = (7 - 8)GM$ which for an assumed mass of $1.4M_\odot$ results in $R < 14.5 - 16.5$ km (see Fig. 1.9). Limits on the compactness, the mass-to-radius (M/R) ratio, can be extracted rather model independent from the profile of thermal x-rays emitted from hot spots on the surface of weakly magnetized millisecond pulsars as demonstrated in [83, 84]. For the pulsar J0030+0451 the neutron star must have $R/R_s > 2.3$ which for $M = 1.4M_\odot$ demands for a radius of $R > 9.5$ km.

A certain class of binary neutron stars emits quasi-periodic oscillations and are dubbed therefore QPOs. The neutron star is accreting material from a companion star which causes these oscillations. General Relativity predicts that there exists an innermost stable circular orbit (ISCO) which for a spherical system is given by $R_{\text{isco}} = 3R_s = 6GM$ in the Schwarzschild-metric when effects from the rotation of the neutron star can be neglected. If an innermost stable circular orbit of these accreting systems can be detected the radius of the neutron star has to be lower than this limit providing a rather stringent constraint on the properties of neutron stars. The highest QPO frequency measured so far is for the system 4U 0614+091 with a frequency of 1330 Hz [85]. A stable circular orbit within the Schwarzschild metric is given by $\Omega^2 = M/r^3$. The radius of the neutron star has to be lower than that giving the constraint

$$R \leq R_{\text{orb}} = \left(\frac{GM}{4\pi^2\nu_{\text{QPO}}^2} \right) \quad (11)$$

where ν_{QPO} is the highest measured QPO frequency. General Relativity demands that the stable circular orbit must be larger than the ISCO, $R_{\text{orb}} \leq R_{\text{isco}}$. The combination of the two conditions cuts out a wedge-like shape in the mass-radius diagram which is bounded by a maximum mass and a corresponding radius. The mass-radius curve for neutron stars has to pass this region [86], see also the mass-radius plot in Fig. 1.9. There have been several claims that indeed the innermost stable circular orbit has been detected, most notably and recently for the QPOs measured for 4U 1636 [87] arriving at a neutron star mass of $2.0M_\odot$. A phase resolved spectroscopy with the VLT recovers a smaller neutron star mass range of 1.6 to $1.9M_\odot$ prevailing any firm conclusion about a massive compact star.

There are rather model independent constraints on the maximum mass possible for neutron stars which rely just on general relativity and causality for the nuclear equation of state. Let us assume that the nuclear equation of state is known up to some fiducial energy density, be it from the measurement of the properties of nuclei or from the determination of the in-medium properties of hadronic matter as generated in heavy-ion collisions. Then the high-density equation of state above that fiducial energy density can be limited by demanding that the hydrodynamical speed of sound can not exceed the speed of light. For the simplest case this criterion reads for the equation

of state that

$$p = c_s^2 \epsilon \quad \text{with} \quad c_s^2 \leq c^2 \quad . \quad (12)$$

Even if the nuclear equation of state is unknown above some energy density, the pressure can not rise more rapidly than given by the limiting case $p = \epsilon$, i.e. the nuclear equation of state can not be stiffer than that due to causality. In turn, the stiffest possible equation of state provides the maximum possible mass configurations for compact stars, as it gives for a given energy density the maximum possible pressure which can counterbalance the pull of gravity. Now one can assume that one knows the nuclear EoS up to some fiducial energy density. For higher energy densities one adopts the stiffest possible equation of state. The resulting maximum mass is the highest neutron star mass allowed by causality and by the nuclear EoS fixed up to a certain energy density. There exists scaling relations for the TOV equations. It can be shown that the maximum possible mass scales in the following way with the fiducial energy density ϵ_f where one switches from the nuclear EoS to the stiffest possible EoS:

$$M_{\max} = 4.2 M_{\odot} \left(\frac{2.5 \cdot 10^{14} \text{ g cm}^{-3}}{\epsilon_f} \right)^{1/2} \quad (13)$$

where $\epsilon_0 = m_N \cdot n_0 = 2.5 \cdot 10^{14} \text{ g cm}^{-3}$ corresponds to a nuclear (number) density of $n_0 = 0.16 \text{ fm}^{-3}$. The prefactor of $4.2 M_{\odot}$ is determined numerically and depends on the nuclear EoS adopted. There exists several investigations on this maximum mass constraint using a different nuclear EoS which come to about similar numerical values for the maximum mass [88, 89, 90, 91]. Note that the nuclear EoS utilized in these works are constrained by nucleon-nucleon interactions and the properties of nuclei, so the nuclear EoS is probed only up to normal nuclear matter density. Usually, a higher fiducial energy density is given, about twice the normal value, which is unjustified and would result in a maximum mass constraint of around $3 M_{\odot}$, which is actually the standard value quoted in the literature. We argue that the nuclear EoS can not be reliably fixed from the properties of the nucleon-nucleon interaction and of nuclei above normal nuclear density at present so that the correct mass limit from nuclear models is given by about $4.2 M_{\odot}$. The determination of the nuclear EoS at supranuclear densities as done with subthreshold kaon production gives tighter constraints on the maximum mass, as the fiducial density can be increased to about 2 to 2.5 times normal nuclear matter density, so that the maximum possible mass for a neutron star would be limited to about $2.7 - 3.0 M_{\odot}$.

In addition, there is another ingredient to the nuclear EoS for neutron stars which is difficult to determine at present: the density dependence of the nuclear asymmetry energy (for a recent review on the role of the asymmetry energy for nuclei and neutron stars see [92]). It is noteworthy, that there seems to be a general trend for the mass-radius relation of compact stars for modern realistic nuclear equation of states. The lower end of the neutron star branch is determined by the rather well known low-density equation of state and is located around a mass of $0.1 M_{\odot}$ and a radius of about 250 km (see e.g. [93, 94]). The maximum density is just above the critical density for the onset of homogeneous neutron star matter, about half normal nuclear matter density. As the neutron star material consists of a lattice of nuclei immersed in a gas of electrons and (free but interacting) neutrons below that density, the neutron star is mainly solid not liquid. The low-density equations of state are usually taken from [93, 95], see [96] for an update of the so called BPS equation of state [93]. At one to three times normal nuclear matter density, interactions start to give a sizable contribution to the pressure. The resulting equation of state can be approximated by a polytrope of the form $p \sim n^2 \sim \epsilon^2$. The exact critical density where the overturn happens is controlled by the strength and the density dependence of the asymmetry energy. The mass-radius relation for a polytrope of the above form is well known and quite simple: the radius becomes independent of the central density and therefore of the mass of the neutron star. Indeed, one finds in more sophisticated approaches, that the mass increases drastically between a rather narrow window in radius of typically 10 to 15 km, see the reviews [97, 75]. Common nonrelativistic approaches to the

neutron star matter equation of state have lower radii than relativistic approaches, as the density dependence of the asymmetry energy in relativistic models is generically much stronger than in the nonrelativistic ones. The observation of the relation between the radius of a neutron star and the asymmetry energy led to the idea to determine the asymmetry energy by measuring the neutron radius of led to learn something about the mass-radius relation of neutron stars [98]. However, we point out that the central density for neutron star masses observed so far are well above normal nuclear matter density. One needs actually to know the asymmetry energy at about three times normal nuclear matter density. This density regime could be reached by heavy-ion collisions at a few GeV bombarding energy, where particle ratios as the subthreshold K^-/K^+ ratio [99] or the π^-/π^+ ratio measured with the FOPI spectrometer [100, 101] could serve as a probe of the isospin dependent forces at high densities.

At high densities the nuclear equation of state is not only essentially unknown but also the overall composition and structure could be totally different. New exotic particles and phases can appear which alter not only the global properties of compact stars, the total mass and radius, but also the cooling evolution and the stability against the emission of gravitational waves or the delayed collapse to a black hole.

Many different model approaches predict that hyperons are present in neutron star matter around twice normal nuclear matter density. The composition of hyperons depends crucially on the hyperon-nucleon interactions, in particular on the hyperon self-energies. Hyperons can be abundantly present so that a neutron star is in this case more aptly dubbed a 'giant hypernucleus' [102]. The impacts of hyperons on the properties is manifold. Most importantly, the maximum possible mass is drastically reduced, even when many-body effects and a repulsive interactions between hyperons are taken into account [103]. If there is a phase transition to hyperon-rich matter in the core of neutron stars, a new stable branch in the mass-radius curve can be present which are compact stars with similar radii but smaller radii [104]. But also the cooling is affected as hyperons open new additional cooling processes which are controlled by the hyperon-hyperon interactions. Hypernuclear experiments measuring double hypernuclei at J-PARC and at the PANDA experiment at FAIR, GSI Darmstadt will shed more light on the strength of the hyperon-hyperon interactions in the near future. Bound states of hyperons could be formed in relativistic heavy-ion collisions as dozens of hyperons are produced in a single event (see e.g. [105]). The study of those systems will be crucial in determining the hyperon-hyperon interaction and the hyperon composition of neutron stars in the interior. For a review on the relation between hypernuclear physics and neutron stars see [106].

Around three to four times normal nuclear matter density another sort of strange hadron could be present in the dense interior of compact stars: Antikaons which form a Bose condensate. Antikaons are formed in beta-stable matter by transforming electrons to negatively charged antikaons, $e^- \rightarrow K^- + \nu_e$, where the neutrino is emitted and acts as an additional cooling agent [108]. The loss of electron pressure and the nonexistent pressure contribution from the Bose condensate destabilizes the compact star matter so that the maximum mass of neutron stars is drastically reduced giving rise to stellar mass black holes, the Bethe-Brown scenario [109]. Crucial input to the scenario of antikaon condensation is the highly attractive potential felt by antikaons in dense matter, a scenario which can be probed by subthreshold production of antikaons in relativistic heavy-ion collisions as measured by the KaoS collaboration [110, 111, 112]. For the imminent correlation between antikaon condensation and antikaon production in heavy-ion collisions see [113, 114]. The in-medium potential of antikaons can not be reliably extracted from the production rates, as matter produced in heavy-ion collisions has different properties than neutron star matter as (see e.g. [115] for a detailed investigation on this point). The strong in-medium potentials for antikaons also enhances the in-medium cross section so that the production rates saturate. The correlated emission of antikaons might serve as a better observable to probe the in-medium potential of antikaons. We point out again that the subthreshold production of kaons (K^+) is an excellent tool for constraining the nuclear equation of state above normal nuclear matter saturation density as discussed above in more detail. However, in contrast to antikaons the K^+ feels a repulsive potential

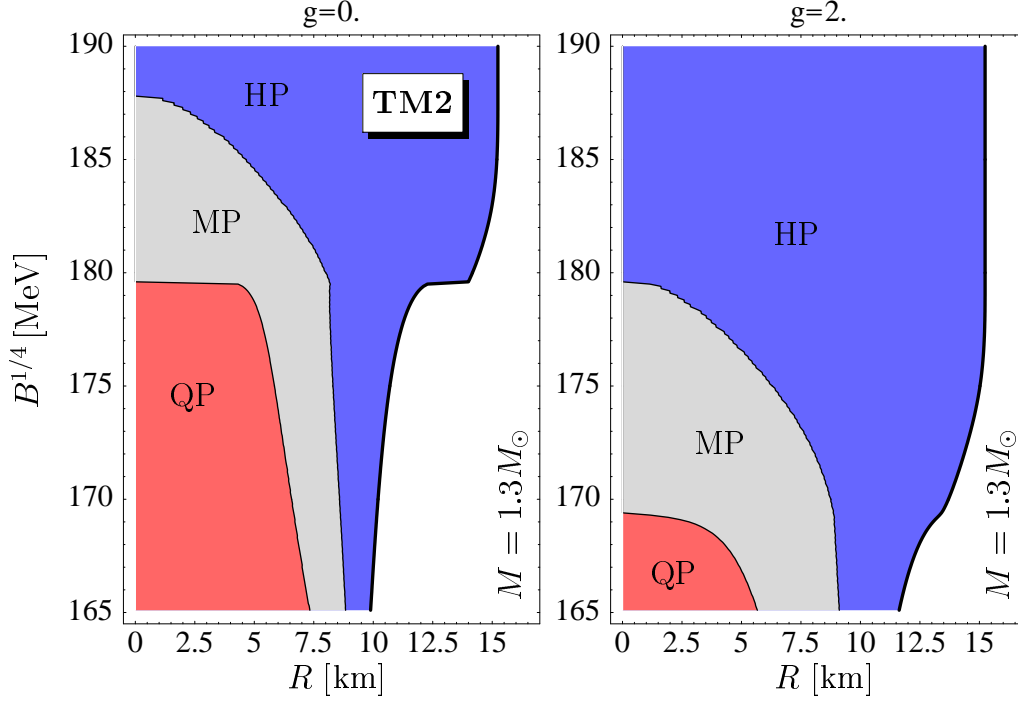


Figure 1.10: Cut through a neutron star with quark matter for different values of the MIT bag constant without (left plot) and with corrections from a hard dense loop calculation (right plot). The figure is taken from [107]. QP: Quark phase, MP: Mixed phase, HP: Hadronic phase.

in dense matter so that kaons are unlikely to be present in neutron star matter.

Finally, the extreme densities in the core of neutron stars can reach the point in the QCD phase diagram where matter is converted from the hadronic chirally broken phase to the chirally restored quark matter phase (here for simplicity we denote the new phase as being quark). The phase transition to quark matter in compact star matter can have profound consequences for the physics of neutron stars and core-collapse supernovae. The physics of strange quark matter and quark stars have been reviewed in [116]. Many signals for the presence of quark matter and the QCD phase transition have been proposed in the literature also for explosive processes in astrophysics as for gamma-ray bursts, gravitational wave emission from neutron star mergers (for a recent review we refer to [117]). The amount of quark matter in the core of compact stars is still an open question and best illustrated in Fig. 1.10.

The astrophysical constraints on the nuclear equation of state and the quark matter equation of state have been investigated in more detail in [118, 119] including also observables from heavy-ion experiments. Some of the astrophysical input data has been revised in the mean-time and some can not be taken as serious constraints as discussed above. If limits from astrophysical data are taken firmly and as proposed in the literature, in particular if one assumes a maximum mass of a neutron star of $2M_\odot$ or more, then it turns out that none of the purely hadronic equation of state can fulfill all the constraints imposed. This finding points to two important statements: astrophysical data can indeed give strong constraints on the nuclear equation of state but it has to be taken with great caution. In the near future with the advent of new detectors one will get a much tighter grip on the properties of the nuclear equation of state at high densities from astrophysical observations.

1.4 References

- 1 H.A. Gustafsson et al., Phys. Rev. Lett **52**, 1590 (1984)
- 2 R. Stock et al., Phys. Rev. Lett. **49**, 1236 (1982)
- 3 A.E.S. Green, Phys. Rep. **95**, 1006 (1954)
- 4 R. Mattuck, A Guide to Feynman Diagrams in the Many-Body Problem, McGraw-Hill Publishing, London
- 5 M. Baldo et al. , Phys. Rev. **C41**, 1748 (1990).
- 6 R. Brockmann and R. Machleit, Phys. Rev. **C42**, 1965 (1990).
- 7 K.A. Brückner Phys. Rev. **97**, 1353 (1955)
- 8 M. Baldo and C. Maieron, *J. Phys. G* **34** R243, (2007).
- 9 C. Fuchs, H. H. Wolter, *Euro. Phys. J. A* **30**, 5 (2006).
- 10 C. Fuchs, PoS C **POD07** (2007) 060 [arXiv:0711.3367 [nucl-th]].
- 11 P. Danielewicz, AIP Conference Proceedings **597**, (2001) 24-42, arXiv:nucl-th/0112006
- 12 D.H. Youngblood, H.L. Clark and Y.-W. Lui, Phys. Rev. Lett **84** (1999) 691.
- 13 J. Piekarewicz, Phys. Rev. **C69** (2004) 041301 and references therein.
- 14 S. Shlomo, V.M. Kolomietz and G. Colo, Eur. Phys. J. A30, 23 (2006)
- 15 G. Colo, N. Van Giai, J. Meyer, K. Bennaceur , P. Bonche Phys.Rev. **C70**, 024307 (2004), nucl-th/0403086
- 16 D. Vretenar, T. Niksic, P. Ring Phys.Rev. **C68** ,024310 (2003), nucl-th/0302070
- 17 M.M. Sharma arXiv:0811.2729
- 18 C. Hartnack et al., Eur. Phys. J. **A1** (1998) 151.
- 19 S. A. Bass et al. Prog. Part. Nucl. Phys. **41** (1998) 225
- 20 J. Aichelin, Phys. Reports **202**, 233 (1991).
- 21 W. Cassing et al., Nucl. Phys. **A614** (1997) 415; W. Cassing and E. Bratkovskaya, Phys. Rep. **308** (1999) 65.
- 22 C. Fuchs et al., Phys. Lett **B 434** (1998) 245 ; C. Fuchs et al., Phys. Rev. Lett **86** (2001) 1794; C. Fuchs et al., J. Phys. G **28** (2002) 1615
- 23 H. Stöcker and W. Greiner, Phys. Reports **137**, 277 (1986).
- 24 A. Andronic et al., Phys. Lett. **B612** (2005) 173.
- 25 E.E. Kolomeitsev, C. Hartnack, H.W. Barz, M. Bleicher, E. Bratkovskaya, W. Cassing, L.W. Chen, P. Danielewicz, C. Fuchs, T. Gaitanos, C.M. Ko, A. Larionov, M. Reiter, Gy. Wolf, J. Aichelin, J. Phys. G **31** (2005) 741.
- 26 Christian Fuchs, Prog.Part.Nucl.Phys. **56**, 1(2006)

-
- 27 C. Hartnack, H. Oeschler and J. Aichelin, Phys. Rev. Lett. **96** (2006) 012302.
 - 28 C.L. Korpa and M.F.M. Lutz, Acta Phys. Hung. **A22** (2005) 21 nucl-th/0404088; M.F.M. Lutz and C.L. Korpa, Nucl. Phys. **A700** (2002) 309
 - 29 J. Randrup and C.M. Ko, Nucl. Phys. A **343**, 519 (1980).
 - 30 K. Tsushima et al., Phys. Lett. **B337** (1994) 245; Phys. Rev. **C 59** (1999) 369 (nucl-th/9801063)
 - 31 C. Sturm et al., (KaoS Collaboration), Phys. Rev. Lett. **86** (2001) 39.
 - 32 H. A. Bethe and R. Wilson, James, Astrophys. J. **295**, 14 (1985).
 - 33 H.-T. Janka, R. Buras, F. S. Kitaura Joyanes, A. Marek, M. Rampp and L. Scheck, Nucl. Phys. **A758**, 19 (2005), [astro-ph/0411347].
 - 34 R. Buras, H.-T. Janka, M. Rampp and K. Kifonidis, Astron. Astrophys. **457**, 281 (2006), [astro-ph/0512189].
 - 35 A. Burrows, E. Livne, L. Dessart, C. Ott and J. Murphy, Astrophys. J. **640**, 878 (2006), [astro-ph/0510687].
 - 36 A. Marek, H. T. Janka and E. Mueller, 0808.4136.
 - 37 H. Dimmelmeier, C. D. Ott, A. Marek and H.-T. Janka, Phys. Rev. D **78**, 064056 (2008), [0806.4953].
 - 38 H.-T. Janka, K. Langanke, A. Marek, G. Martínez-Pinedo and B. Müller, Phys. Rept. **442**, 38 (2007), [astro-ph/0612072].
 - 39 S. Rosswog, M. Liebendörfer, F.-K. Thielemann, M. B. Davies, W. Benz and T. Piran, Astron. Astrophys. **341**, 499 (1999), [arXiv:astro-ph/9811367].
 - 40 S. Rosswog, M. B. Davies, F.-K. Thielemann and T. Piran, Astron. Astrophys. **360**, 171 (2000), [arXiv:astro-ph/0005550].
 - 41 R. Oechslin, H.-T. Janka and A. Marek, Astron. Astrophys. **467**, 395 (2007), [astro-ph/0611047].
 - 42 R. Oechslin and H. T. Janka, Phys. Rev. Lett. **99**, 121102 (2007), [astro-ph/0702228].
 - 43 S. Rosswog, R. Speith and G. A. Wynn, Mon. Not. R. Astron. Soc. **351**, 1121 (2004), [arXiv:astro-ph/0403500].
 - 44 S. Rosswog, Last Moments in the Life of a Compact Binary System: Gravitational Waves, Gamma-Ray Bursts and Magnetar Formation, in *Revista Mexicana de Astronomia y Astrofisica*, vol. 27, , Revista Mexicana de Astronomia y Astrofisica, vol. 27 Vol. 27, pp. 57–79, 2007.
 - 45 J. M. Lattimer and F. D. Swesty, Nucl. Phys. **A535**, 331 (1991).
 - 46 H. Shen, H. Toki, K. Oyamatsu and K. Sumiyoshi, Nucl. Phys. **A637**, 435 (1998), [nucl-th/9805035].
 - 47 R. Oechslin, K. Uryū, G. Poghosyan and F. K. Thielemann, Mon. Not. R. Astron. Soc. **349**, 1469 (2004).
 - 48 N. A. Gentile, M. B. Aufderheide, G. J. Mathews, F. D. Swesty and G. M. Fuller, Astrophys. J. **414**, 701 (1993).

-
- 49 N. Yasutake, K. Kotake, M.-a. Hashimoto and S. Yamada, Phys. Rev. D **75**, 084012 (2007), [astro-ph/0702476].
 - 50 K. Nakazato, K. Sumiyoshi and S. Yamada, Phys. Rev. **D77**, 103006 (2008), [0804.0661].
 - 51 I. Sagert, M. Hempel, G. Pagliara, J. Schaffner-Bielich, T. Fischer, A. Mezzacappa, F.-K. Thielemann and M. Liebendorfer, arXiv:0809.4225 [astro-ph].
 - 52 R. C. Tolman, *Relativity, Thermodynamics and Cosmology* (Oxford University Press, Oxford, 1934).
 - 53 R. C. Tolman, Phys. Rev. **55**, 364 (1939).
 - 54 J. R. Oppenheimer and G. M. Volkoff, Phys. Rev. **55**, 374 (1939).
 - 55 J. M. Weisberg and J. H. Taylor, The relativistic binary pulsar b1913+16: Thirty years of observations and analysis, in *Binary Radio Pulsars*, edited by F. A. Rasio and I. H. Stairs, , Astronomical Society of the Pacific Conference Series Vol. 328, p. 25, 2005, [astro-ph/0407149].
 - 56 U. H. Gerlach, Phys. Rev. **172**, 1325 (1968).
 - 57 L. Lindblom, Astrophys. J. **398**, 569 (1992).
 - 58 LIGO Scientific, B. Abbott *et al.*, Phys. Rev. **D76**, 042001 (2007), [gr-qc/0702039].
 - 59 I. H. Stairs, J. Phys. G **32**, S259 (2006).
 - 60 D. J. Nice, I. H. Stairs and L. E. Kasian, AIP Conference Proceedings **983**, 453 (2008).
 - 61 R. N. Manchester, G. B. Hobbs, A. Teoh and M. Hobbs, Astronomical Journal **129**, 1993 (2005), [astro-ph/0412641].
 - 62 A. Lyne *et al.*, Science **303**, 1153 (2004), [astro-ph/0401086].
 - 63 S. E. Thorsett and D. Chakrabarty, Astrophys. J. **512**, 288 (1999).
 - 64 A. J. Faulkner *et al.*, Astrophys. J. **618**, L119 (2005), [astro-ph/0411796].
 - 65 D. J. Nice, E. M. Splaver, I. H. Stairs, O. Löhmer, A. Jessner, M. Kramer and J. M. Cordes, Astrophys. J. **634**, 1242 (2005), [astro-ph/0508050].
 - 66 H. Quaintrell, A. J. Norton, T. D. C. Ash, P. Roche, B. Willems, T. R. Bedding, I. K. Baldry and R. P. Fender, Astron. Astrophys. **401**, 313 (2003).
 - 67 S. M. Ransom, J. W. T. Hessels, I. H. Stairs, P. C. C. Freire, F. Camilo, V. M. Kaspi and D. L. Kaplan, Science **307**, 892 (2005), [astro-ph/0501230].
 - 68 P. C. C. Freire, S. M. Ransom, S. Bégin, I. H. Stairs, J. W. T. Hessels, L. H. Frey and F. Camilo, Astrophys. J. **675**, 670 (2008), [0711.0925].
 - 69 P. C. C. Freire, A. Wolszczan, M. van den Berg and J. W. T. Hessels, Astrophys. J. **679**, 1433 (2008), [0712.3826].
 - 70 D. J. Champion *et al.*, Science **320**, 1309 (2008), [0805.2396].
 - 71 J. P. W. Verbiest, M. Bailes, W. van Straten, G. B. Hobbs, R. T. Edwards, R. N. Manchester, N. D. R. Bhat, J. M. Sarkissian, B. A. Jacoby and S. R. Kulkarni, Astrophys. J. **679**, 675 (2008), [0801.2589].

-
- 72 J. E. Trümper, V. Burwitz, F. Haberl and V. E. Zavlin, Nucl. Phys. Proc. Suppl. **132**, 560 (2004), [astro-ph/0312600].
- 73 W. C. G. Ho, Mon. Not. R. Astron. Soc. **380**, 71 (2007), [arXiv:0705.4543 [astro-ph]].
- 74 N. A. Webb and D. Barret, Astrophys. J. **671**, 727 (2007), [arXiv:0708.3816 [astro-ph]].
- 75 J. M. Lattimer and M. Prakash, Phys. Rept. **442**, 109 (2007), [astro-ph/0612440].
- 76 J. Cottam, F. Paerels and M. Mendez, Nature **420**, 51 (2002), [astro-ph/0211126].
- 77 J. Cottam, F. Paerels, M. Mendez, L. Boirin, W. H. G. Lewin, E. Kuulkers and J. M. Miller, Astrophys. J. **672**, 504 (2008), [arXiv:0709.4062 [astro-ph]].
- 78 F. Özel, Nature **441**, 1115 (2006), [astro-ph/0605106].
- 79 K. J. Pearson, R. Hynes, D. Steeghs, P. Jonker, C. Haswell, A. King, K. O’Brien, G. Nelemans and M. Mendez, Astrophys. J. **648**, 1169 (2006), [astro-ph/0605634].
- 80 M. Alford, D. Blaschke, A. Drago, T. Klähn, G. Pagliara and J. Schaffner-Bielich, Nature **445**, E7 (2006), [astro-ph/0606524].
- 81 G. B. Rybicki, C. O. Heinke, R. Narayan and J. E. Grindlay, Astrophys. J. **644**, 1090 (2006), [astro-ph/0506563].
- 82 E. M. Cackett, J. M. Miller, S. Bhattacharyya, J. E. Grindlay, J. Homan, M. van der Klis, M. C. Miller, T. E. Strohmayer and R. Wijnands, Astrophys. J. **674**, 415 (2008), [0708.3615].
- 83 S. Bogdanov, G. B. Rybicki and J. E. Grindlay, Astrophys. J. **670**, 668 (2007), [arXiv:astro-ph/0612791].
- 84 S. Bogdanov, J. E. Grindlay and G. B. Rybicki, 0801.4030.
- 85 S. van Straaten, E. C. Ford, M. van der Klis, M. Méndez and P. Kaaret, Astrophys. J. **540**, 1049 (2000), [arXiv:astro-ph/0001480].
- 86 M. C. Miller, F. K. Lamb and D. Psaltis, Astrophys. J. **508**, 791 (1998), [arXiv:astro-ph/9609157].
- 87 D. Barret, J.-F. Olive and M. C. Miller, Mon. Not. Roy. Astron. Soc. **376**, 1139 (2007), [astro-ph/0701312].
- 88 C. E. Rhoades and R. Ruffini, Phys. Rev. Lett. **32**, 324 (1974).
- 89 J. B. Hartle, Phys. Rep. **46**, 201 (1978).
- 90 V. Kalogera and G. Baym, Astrophys. J. Lett. **470**, L61 (1996), [arXiv:astro-ph/9608059].
- 91 A. Akmal, V. R. Pandharipande and D. G. Ravenhall, Phys. Rev. C **58**, 1804 (1998).
- 92 A. W. Steiner, M. Prakash, J. M. Lattimer and P. J. Ellis, Phys. Rept. **411**, 325 (2005), [nucl-th/0410066].
- 93 G. Baym, C. Pethick and P. Sutherland, Astrophys. J. **170**, 299 (1971).
- 94 J. Macher and J. Schaffner-Bielich, Eur. J. Phys. **26**, 341 (2005), [astro-ph/0411295].
- 95 J. W. Negele and D. Vautherin, Nucl. Phys. **A207**, 298 (1973).
- 96 S. B. Rüster, M. Hempel and J. Schaffner-Bielich, Phys. Rev. C **73**, 035804 (2006), [astro-ph/0509325].

-
- 97 J. M. Lattimer and M. Prakash, *Astrophys. J.* **550**, 426 (2001), [astro-ph/0002232].
 - 98 C. J. Horowitz and J. Piekarewicz, *Phys. Rev. Lett.* **86**, 5647 (2001), [astro-ph/0010227].
 - 99 G. Ferini, T. Gaitanos, M. Colonna, M. Di Toro and H. H. Wolter, *Phys. Rev. Lett.* **97**, 202301 (2006), [nucl-th/0607005].
 - 100 FOPI, W. Reisdorf *et al.*, *Nucl. Phys.* **A781**, 459 (2007), [nucl-ex/0610025].
 - 101 Z. Xiao, B.-A. Li, L.-W. Chen, G.-C. Yong and M. Zhang, 0808.0186.
 - 102 N. K. Glendenning, *Astrophys. J.* **293**, 470 (1985).
 - 103 N. K. Glendenning and S. A. Moszkowski, *Phys. Rev. Lett.* **67**, 2414 (1991).
 - 104 J. Schaffner-Bielich, M. Hanauske, H. Stöcker and W. Greiner, *Phys. Rev. Lett.* **89**, 171101 (2002), [astro-ph/0005490].
 - 105 J. Schaffner-Bielich, R. Mattiello and H. Sorge, *Phys. Rev. Lett.* **84**, 4305 (2000), [nucl-th/9908043].
 - 106 J. Schaffner-Bielich, *Nucl. Phys.* **A804**, 309 (2008), [0801.3791].
 - 107 K. Schertler, C. Greiner, J. Schaffner-Bielich and M. H. Thoma, *Nucl. Phys.* **A677**, 463 (2000), [astro-ph/0001467].
 - 108 G. E. Brown, K. Kubodera, M. Rho and V. Thorsson, *Phys. Lett. B* **291**, 355 (1992).
 - 109 G. E. Brown and H. A. Bethe, *Astrophys. J.* **423**, 659 (1994).
 - 110 R. Barth *et al.* (KaoS Collaboration), *Phys. Rev. Lett.* **78**, 4007 (1997).
 - 111 KaoS, C. Sturm *et al.*, *Phys. Rev. Lett.* **86**, 39 (2001), [nucl-ex/0011001].
 - 112 A. Forster *et al.*, *Phys. Rev. C* **75**, 024906 (2007), [nucl-ex/0701014].
 - 113 G. Q. Li, C.-H. Lee and G. E. Brown, *Phys. Rev. Lett.* **79**, 5214 (1997).
 - 114 G.-Q. Li, C. H. Lee and G. E. Brown, *Nucl. Phys.* **A625**, 372 (1997), [nucl-th/9706057].
 - 115 J. Schaffner-Bielich, V. Koch and M. Effenberger, *Nucl. Phys.* **A669**, 153 (2000).
 - 116 F. Weber, *Prog. Part. Nucl. Phys.* **54**, 193 (2005), [astro-ph/0407155].
 - 117 J. Schaffner-Bielich, *PoS (CPOD2007)*, 062 (2007), [arXiv:0709.1043 [astro-ph]].
 - 118 T. Klähn *et al.*, *Phys. Rev. C* **74**, 035802 (2006), [nucl-th/0602038].
 - 119 T. Klähn, D. Blaschke, F. Sandin, C. Fuchs, A. Faessler, H. Grigorian, G. Röpke and J. Trümper, *Phys. Lett.* **B654**, 170 (2007), [nucl-th/0609067].